ASSEMBLY OF BACTERIOPHAGE T7

DIMENSIONS OF THE BACTERIOPHAGE AND ITS CAPSIDS

ROBERT M. STROUD, PHILIP SERWER, AND MICHAEL J. ROSS, *Department of Biochemistry and Biophysics, University of California School of Medicine, San Francisco, California 94143*

ABSTRACT The dimensions of bacteriophage T7 and T7 capsids have been investigated by small-angle x-ray scattering. Phage T7 behaves like a sphere of uniform density with an outer radius of 301 ± 2 Å (excluding the phage tail) and a calculated volume for protein plus nucleic acid of $1.14 \pm 0.05 \times 10^{-16}$ ml. The outer radius determined for T7 phage in solution is ~30% greater than the radius measured from electron micrographs, which indicates that considerable shrinkage occurs during preparation for electron microscopy. Capsids that have a phagelike envelope and do not contain DNA were obtained from lysates of T7-infected *Escherichia coli* (capsid II) and by separating the capsid component of T7 phage from the phage DNA by means of temperature shock (capsid IV). In both cases the peak protein density is at a radius of 275 Å; the outer radius is 286 ± 4 Å, ~5% smaller than the envelope of T7 phage. The thickness of the envelope of capsid II is 22 ± 4 Å, consistent with the thickness of protein estimated to be 23 ± 5 Å in whole T7 phage, as seen on electron micrographs in which the internal DNA is positively stained. The volume in T7 phage available to package DNA is estimated to be $9.2 \pm 0.4 \times 10^{-17}$ ml. The packaged DNA adopts a regular packing with 23.6 Å interplanar spacing between DNA strands. The angular width of the 23.6 Å reflection shows that the mean DNA-DNA spacing throughout the phage head is 27.5 ± <2.2 Å. A T7 precursor capsid (capsid I) expands when pelleted for x-ray scattering in the ultracentrifuge to essentially the same outer dimensions as for capsids II and IV. This expansion of capsid I can be prevented by fixing with glutaraldehyde; fixed capsid I has peak density at a radius of 247 Å, 10% less than capsid II or IV.

INTRODUCTION

DNA bacteriophages consist of shell of protein subunits arranged to form a polyhedron that encloses the DNA genome, a tubular tail assembly, and tail fibers for attachment to host bacteria. The length of the DNA is 300–500 times the diameter of the head (Tikchonenko, 1969) and the DNA is packaged within the head during the morphogenesis of the bacteriophage.

All the double-stranded DNA bacteriophages studied appear to assemble a DNA-free capsid (procapsid) that subsequently packages DNA; the procapsid undergoes changes in structure and composition before and/or during packaging of DNA (reviewed in Casjens and King, 1975; Murialdo and Becker, 1978; Wood and King, 1979; Earnshaw and Casjens, 1980). Details of bacteriophage T7 are shown in Figs. 1 and 2. The transitions observed

---

Dr. Serwer's present address is Department of Biochemistry, University of Texas, Health Science Center, San Antonio, Tex. 78284. Dr. Ross's present address is Genentech Corp., San Francisco, Calif. 94080.

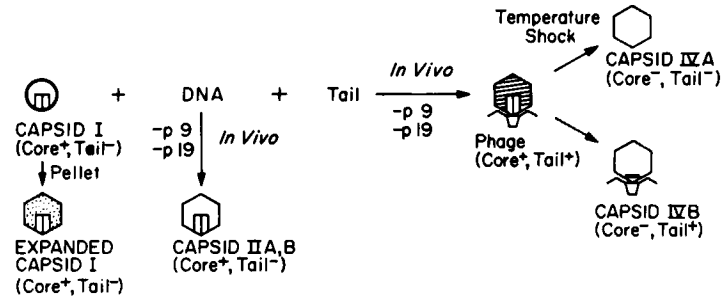

FIGURE 1 Phage T7 capsids. The phage T7 capsids to be analyzed are shown in schematic form. Transformations from one type of capsid to another that occur inside of the phage-infected cell are labeled *in vivo*. Changes induced in the laboratory are labeled with a treatment that produced the change (Serwer, 1976; see Materials and Methods). The presence of a core, tail, or large quantities of P9 is indicated. The further fractionation of capsid II described in Serwer (1981) and Serwer and Watson (1981) is not indicated and was not performed in the present study.

include an increase in the internal volume of the capsid; data suggesting such an increase for bacteriophages T7 (Serwer, 1975), T4 (Steven et al., 1976; Kistler et al., 1978), P22 (Earnshaw et al., 1976), and λ (Earnshaw et al., 1979) have been presented. This observation has suggested that expansion caused a difference in pressure between inside and outside of the T7 capsid that helps push DNA into the capsid during DNA packaging (Serwer, 1975, 1980).

In the studies of T4 and T7 quoted above, the authors relied, at least in part, on dimensions of bacteriophages and bacteriophage capsids determined by electron microscopy and used negative staining to prepare specimens. Negative staining results in a decrease in volume due to dehydration and flattening (probably because of surface tension during drying) of bacteriophages (Serwer, 1977; Earnshaw et al., 1978*a*). Small angle x-ray scattering does not dry the specimen and is, therefore, a more reliable technique than electron microscopy for obtaining dimensions (Guinier and Fournet, 1955; Anderegg et al., 1961, 1963; Harrison, 1969; Jack and Harrison, 1975).

Studies of bacteriophage T7 using high angle x-ray diffraction revealed a peak at a spacing of 23.6 Å, which was attributed to the interplanar spacing of packaged DNA (North and Rich, 1961). The width at half-height of this reflection is determined by the ordering of DNA within the phage head. Although usually the width has been interpreted in terms of a mean domain size for a perfect DNA lattice (North and Rich, 1961; Earnshaw et al., 1976; Earnshaw and Harrison, 1977), it is useful to consider the order in terms of a disordered lattice throughout the entire phage volume. The resulting DNA-DNA spacings therefore give a maximum value for the variation in this spacing. (We ignore all other effects of DNA curvature, dislocations, etc., which would also contribute to broadening.)

MATERIALS AND METHODS

Phage and Bacterial Strains

Wild-type bacteriophage T7 and T7 amber mutant 28, mutant in gene 5 (to be referred to as a 5 Am mutant) (Studier, 1969), were kindly provided by Dr. F. W. Studier (Brookhaven National Laborato-

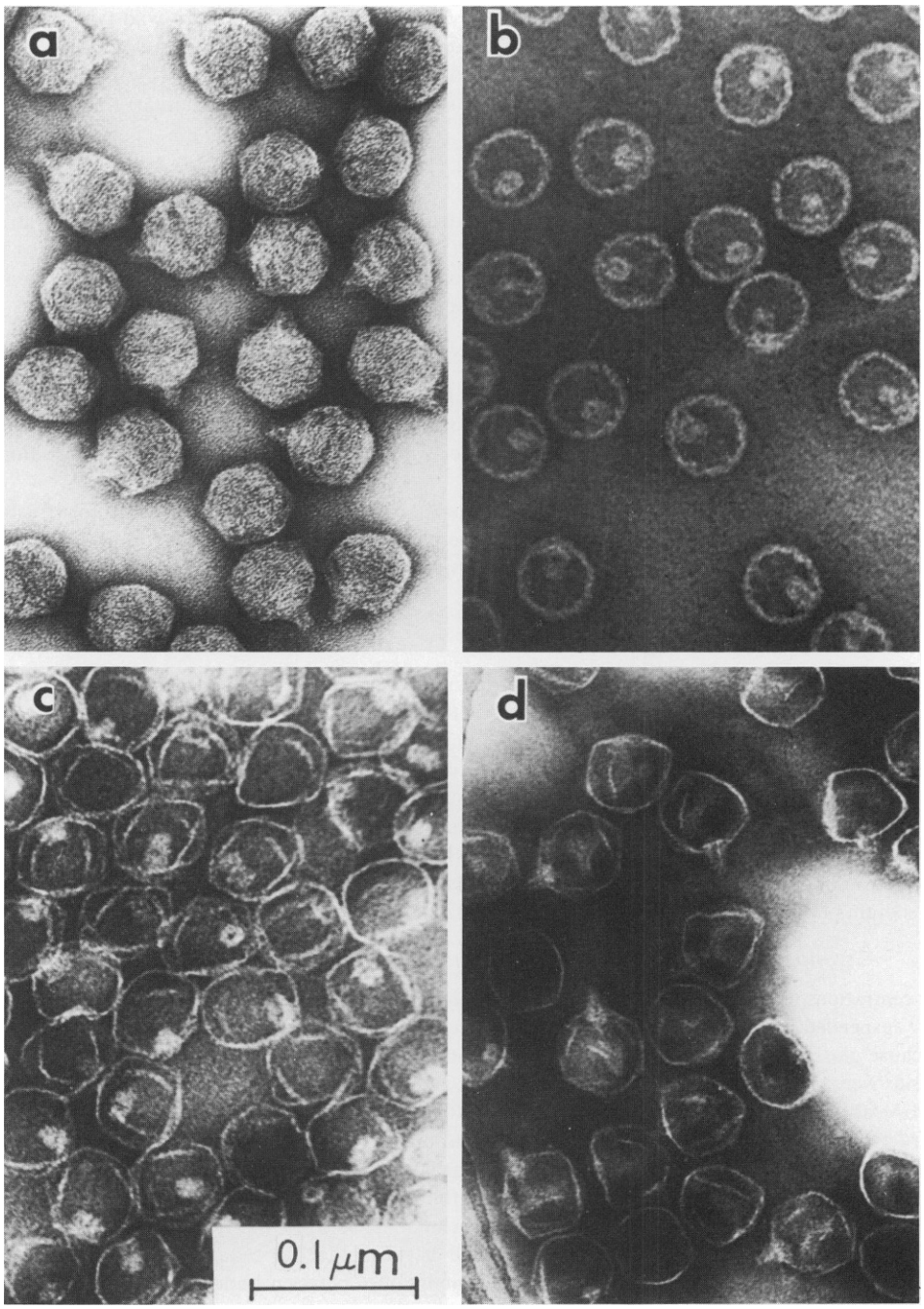

FIGURE 2 Electron microscopy of T7 phage and capsids. (*a*) T7 phage, (*b*) capsid I (from wild-type lystate), (*c*) capsid II, (*d*) capsid IVB.

ries). Gene 5 codes for T7 DNA polymerase and 5 Am mutants infecting a nonpermissive host do not synthesize DNA (Adler and Modrich, 1979; Hori et al., 1979), but do synthesize capsid I (Studier, 1972; Roeder and Sadowski, 1977; Serwer, 1980). *E. coli* BB/1 was the host for wild-type T7 and was the nonpermissive host do not synthesize DNA (Adler and Modrich, 1979; Hori et al., 1979), but do synthesize capsid 1 (Studier, 1972; Roeder and Sadowski, 1977; Serwer, 1980). *E. coli* BB/1 was the host for wild-type T7 and was the nonpermissive host for the amber mutant. *E. coli* O-11′ was the permissive host for the amber mutant.

Media and Buffers

Stocks of wild-type T7 phage were grown in M9 medium (Kellenberger and Séchaud, 1957) at 30°C. Stocks of the amber mutant were grown in T broth (10 g tryptone, 5 g NaCl, 10 liters of water) at 30°C. Buffers used were: (*a*) Tris/Mg buffer: 0.2 M NaCl, 0.01 M Tris, pH 7.4, 0.001 M $MgCl_2$; and (*b*) Phos/Mg buffer: 0.2 M NaCl, 0.01 M sodium phosphate, pH 7.2, 0.001 M $MgCl_2$.

Preparation of T7 Phage and Capsids

Lysates were prepared as follows: an overnight culture of *E. coli* BB/1 in M9 plus 2% T broth was diluted 1:100 into 15 liters of M9 medium. The culture was grown with aeration to 3–4 × 10^8 bacteria/ml, and was then infected with phage. For wild-type phage the multiplicity of infection was 0.05–0.1 and for mutants the multiplicity was 10.

Phage T7 and T7 capsids were precipitated from the lysates with polyethylene glycol (Carbowax 6,000, Union Carbide Corp., New York) and were purified by sedimentation in cesium chloride step gradients, cesium chloride buoyant density gradients, and sucrose gradients, as described in Serwer (1976).

Electron Microscopy

T7 phage and capsids were prepared for electron microscopy as previously described (Serwer, 1976), except when testing pelleting-induced expansion. For such samples a 3-μl aliquot was taken from a sucrose gradient and mixed with 1 μl of 12.5% glutaraldehyde in 0.5 M sodium phosphate, pH 7.2. After 5–10 min at room temperature, the fixed capsids were layered on 5.2 ml of Phos/Mg buffer in a cellulose nitrate centrifuge tube of a Beckman SW50.1 rotor (Beckman Instruments, Inc., Spinco Div., Palo Alto, Calif.); the sample sank to the bottom. Fixed and unfixed samples of the same material were pelleted (30 k, 16 h, 4°C), resuspended in 20 μl of Phos/Mg buffer, and a 3-5-μl droplet of sample was placed on an electron microscope grid for 1 min. The grid was washed with four drops of water and two drops of 1% sodium phosphotungstate, pH 7.6, and dried with filter paper.

Sample Preparation for X-ray Diffraction

Concentrations of samples used for x-ray diffraction were between 5 and 500 mg/ml. Unfixed samples were suspended in Tris/Mg buffer; samples fixed in glutaraldehyde were suspended in Phos/Mg buffer (because glutaraldehyde reacts with Tris buffer and induces a lowering of the pH). Concentrations of capsids were determined by the method of Lowry et al. (1951); phage T7 concentrations were estimated by UV absorbance (Bancroft and Freifelder, 1970). To obtain the high concentrations needed for diffraction, samples were concentrated by sedimentation at 100,000 *g* for 24 h (4°C), the supernate was withdrawn to a known volume, and the resulting pellet was resuspended for 24 h. Phage and capsids subjected to this treatment were examined by electron microscopy. No detectable alteration was found after pelleting with the exception of Capsid 1 (see below).

Solutions for x-ray investigation were contained between the flat cellulose acetate windows of a plexiglass sample holder. Sample temperature was maintained between 1 and 5°C throughout.

X-ray Data Collection

X-ray scattering was recorded on Kodak "no-screen" x-ray film (Eastman Kodak Co., Rochester, N.Y.). The x-ray source was an Elliot GX6 rotating anode generator operating at 500–1,000 W (Elliot—Automation Radar Systems, Ltd., Neutron Div., Borehamwood, Hertfordshire, England) with

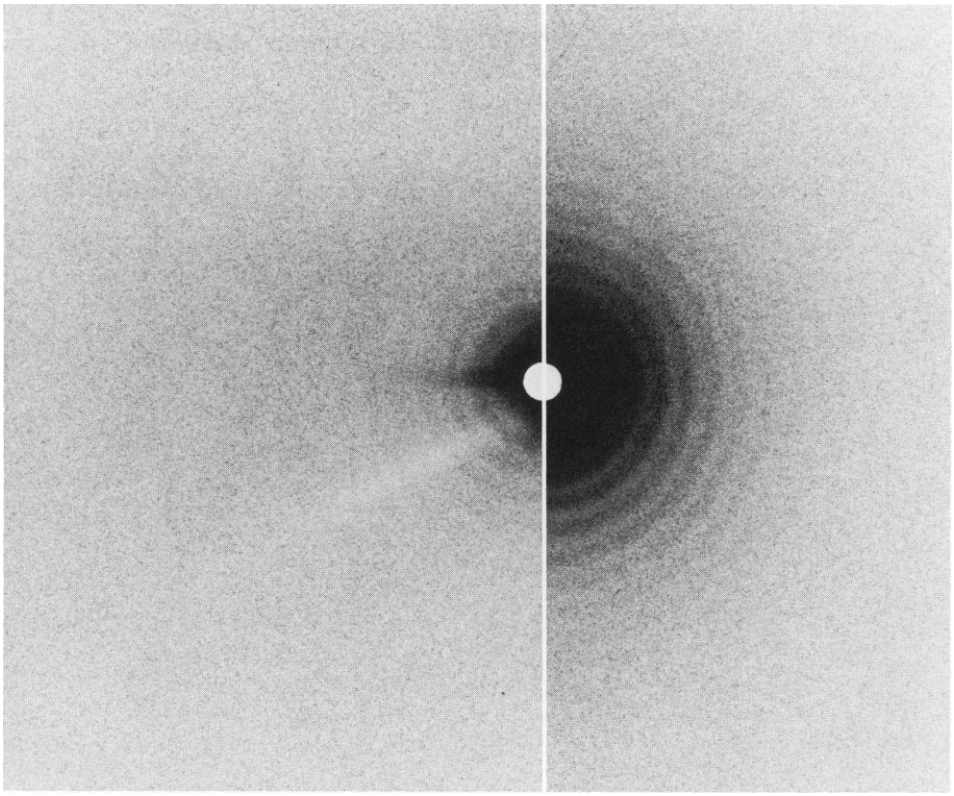

FIGURE 3 Diffraction patterns for T7 capsid II. The pattern on the right is a 77-h exposure of a 50% solution of capsid II. The pattern on the left is recorded from an 11-h exposure of the same solution.

a 100-μm focus. Nickel-filtered Cu Kα radiation was doubly focused with elliptically bent fused silica flats that focused in both the horizontal and vertical planes. The incident beam was always focused onto the film plane, and the focused beam cross section (width at half-height) measured from a short exposure of the direct beam was ~300 μm. The sample chamber and film cassette were rigidly held together at a fixed separation by a helium-filled chamber. The direct beam passed through a 1-mm hole in the film center and the beam stop was behind the film. About five exposures, ranging in time from 1 to 120 h, were used to record the entire small-angle pattern for each structure. Short-term exposures used to record low-order scattering were made from more dilute solutions (<10 mg/ml) to avoid effects of interparticle inteference. Multiple film packs were not used when analyzing data extremely close to the direct beam, since we observed parasitic scattering in this region (corresponding to $1/s > 400$ Å) that was traced to the presence of multiple films. Diffraction recorded for capsid II is shown in Fig. 3.

The effective camera length was determined by dusting the front surface window of the sample holder with talc after each exposure, and recording the talc diffraction pattern. The primary uncertainty in camera length is therefore due to the position of the scattering center with respect to the front surface, owing to the thickness of the sample (up to ~1.0 mm thick), and is therefore conservatively estimated to be ±0.5 mm, out of a total camera length of ~194 mm (i.e., ±0.25%).

Data Processing

Small-angle films were converted into digitized arrays of optical densities on a Syntex Analytical AD-1 flatbed, moving stage, and automicrodensitometer (Syntex Analytical Instruments, Cupertino, Calif.) (Ross and Stroud, 1977). Scanner spot size and raster were both 32 μm square.

Diffraction rings on the film were radially integrated and displayed as the average value of intensity $h(s)$ vs. s (Fig. 4). Regions of the film containing residual parasitic scatter from the focusing mirrors and guard slits were left out of the integration. To integrate the pattern correctly, it was necessary to accurately determine the diffraction center. This was done by iterative refinement of the film center position with respect to the peak maxima in each quadrant of the film. (Approximate film centers, determined from short exposures of the direct beam, were in error by as much as 120 μm.) This factor is significant, since a centering error of 30 μm introduces considerable artificial smearing of the data on radial integrations. Refined centers were determined to within ± 10 μm.

An iterative method was chosen to deconvolute the beam profile from the diffraction pattern (Mencik, 1974) (Fig. 4). To implement the deconvolution, the beam profile $g(s)$ was numerically convoluted with the observed data $h(s)$ to produce a doubly convoluted profile $h'(s)$. The difference between $h'(s)$ and $h(s)$ was taken as a first approximation of the error introduced by the experimental convolution, and

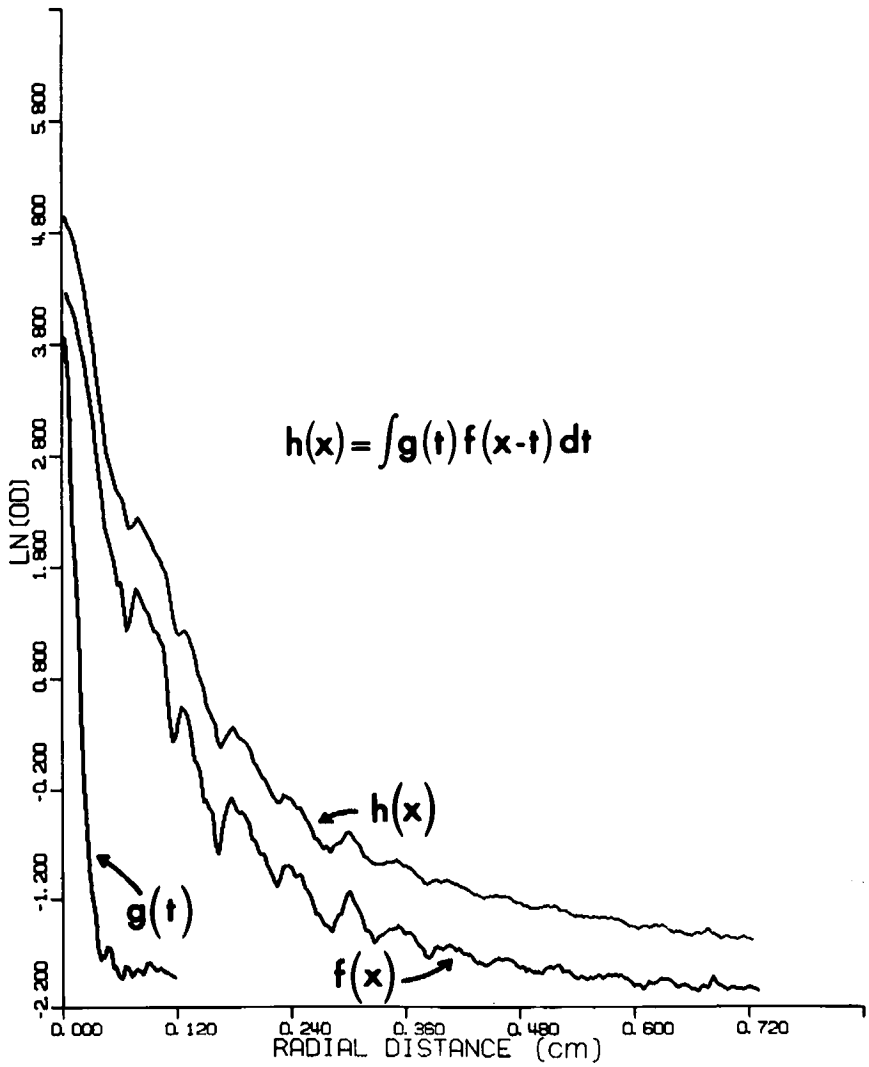

FIGURE 4 The effect of deconvolution. The beam profile $g(s)$ is deconvoluted from the observed data profile $h(s)$. The final result of deconvolution procedure is $f(s)$.

subtracted from $h(s)$ to give a first-order corrected profile $f'(s)$. $f'(s)$ was convoluted with the beam profile and compared with $h(s)$ to obtain a second-order correction. The process was iterated until no improvement in $f(s)$ occurred. The extent of convergence defined as

$$\Delta = \frac{\int_{s=0}^{s_{max}} |f(s)\, g(s) - h(s)|\, ds}{\int_{s=0}^{s_{max}} |h(s)|\, ds}$$

was typically 4% at convergence. The extent of artificial diminution of peak heights that would result if this process were not applied can be seen in Fig. 4.

Multiple exposures were scaled together to give the complete small-angle pattern from $1/s_{min} \sim 600$ Å

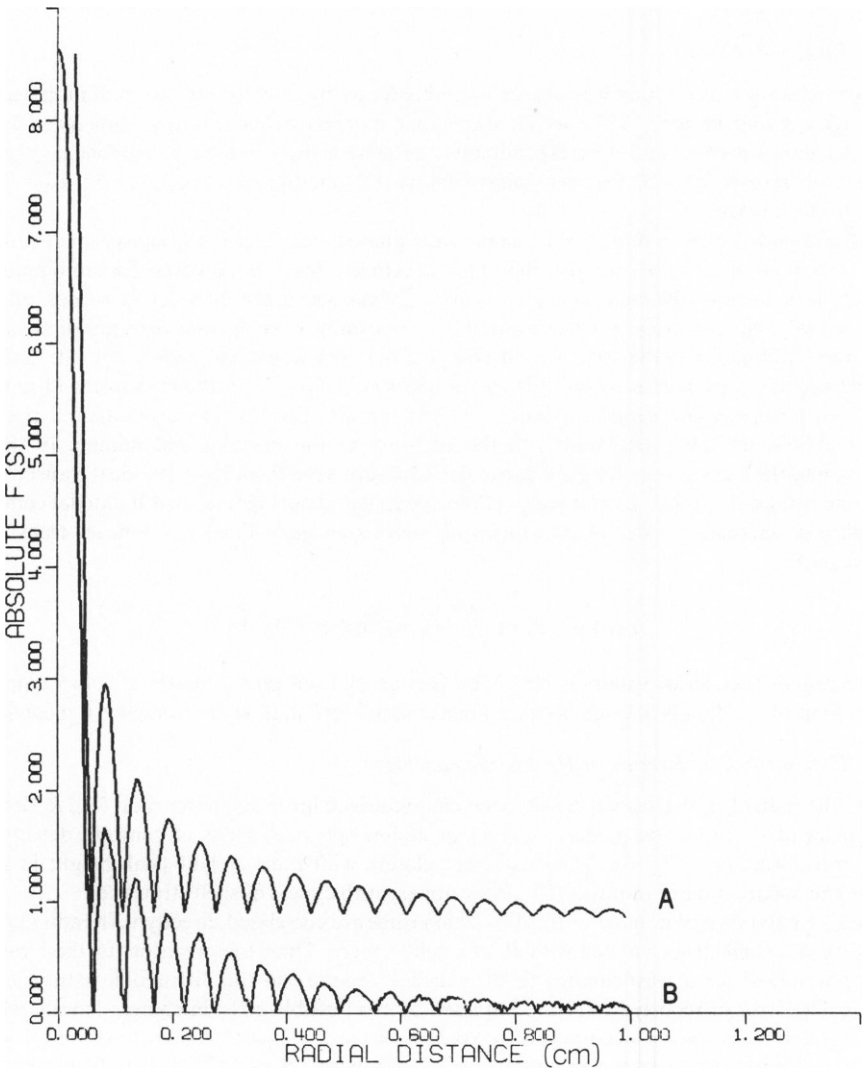

FIGURE 5 A comparison of absolute structure factor profiles for capsid II (curve *B*) and for a perfect shell of inner and outer radii at 263 and 283 Å, respectively (curve *A*). The base line is raised for *A* to simplify comparison.

to $1/s_{max} \sim 20$ Å. The central region of the pattern, unobservable because of interference by the direct beam noise, was determined by extrapolation as follows. Native T7 phage is roughly spherical in the electron microscope and its hydrated DNA component has roughly the same mass density (and therefore electron density) as its hydrated protein (Serwer, 1975). The inner two-thirds of the central maximum was thus estimated from a Guinier plot [ln (h) vs. $\sin^2\theta$] (Guinier and Fournet, 1955). The capsids approximate hollow spherical shells in electron micrographs and linear Guinier plots would not result from the intensity profile of such structures. The unobserved portion of the central maximum of the diffraction pattern from each of these capsids was left out of the initial Fourier synthesis and was iteratively approximated from model structures during the phasing procedure.

A smooth curve through the minima of the deconvoluted diffraction pattern $f(s)$ was subtracted from it since the spherically symmetric harmonics must pass through zeros at minima. The scattering amplitude $F_0(s)$ was calculated as the square root of these deconvoluted and background-subtracted intensities.

Phase Analysis

In favorable cases the diffraction was phased unambiguously by reference to the minimum wavelength principle (Bragg and Perutz, 1952), which states that maxima closer together than Δs = 1/particle radius must have opposite sign. Correspondingly, the spherically symmetric components $G_0(s)$ must contain a true zero $G_0(s) = 0$ between such maxima. Of minima closer than Δs at least one must represent a sign change.

The diffraction patterns from native T7 phage were phased with alternating signs for each maximum (Guinier and Fournet, 1955). For the shell-like structures, there is potential for ambiguity in the interpretation of some of the signs of higher order maxima where the intensity of a peak might drop below noise level, and obscure a true minimum in the transform. In such cases the signs of all successive maxima may alternate, but the signs for all observed maxima would not necessarily alternate. Thus, correct phasing for capsids was established by comparison of $F_0(s)$ with the transforms of model shell structures with appropriate ranges of inner and outer radii (Fig. 5); the experimental positions of maxima and minima were compared with the positions of the maxima and minima in the model transforms, and the signs chosen for each particular structure were those from the ideal transform whose maxima and minima matched most closely. (Coincidentally, phases determined by model comparisons did alternate at successive nodes in transforms of shell structures.) Finally, a Fourier transform was carried out, with

$$\rho(r) = (2/r) \int_{s=0}^{s} F_0(s) \sin(2\pi rs) s \, ds$$

giving the radial electron distribution $\rho(r)$. The portion of each profile inside a radius equal to the resolution limit of the data is omitted because Fourier series termination errors render it meaningless.

Estimation of Errors in Radial Parameters

We report the radii of peak electron density, and characteristic inner and outer radii (R_i, R_o determined by refinement of step-function models (spheres or hollow spherical shells of constant density) to the observed transforms (see Fig. 5). These compare closely with radii at half peak height in $\rho(r)$ and determine the apparent outer radius of T7, or the apparent thickness of shell structures.

The radii of maxima and minima in the diffraction rings are correlated directly with radii $(1/r)$ of the peak density of a shell structure, and with R_o of a solid sphere. Thus, the precision for these radii is the same as determined for a least-squares fit of a model structure to the diffraction pattern (typically $< \pm 0.5$ Å). The error in reported radii is dominated by the possible error in camera length, which was reproducibly measured to an accuracy of $< \pm 0.25\%$ or $\sim \pm 1$ Å (see section above on X-ray Data Collection). Together these errors commute to $< \pm 2$ Å in reported peak radii of shell structures, or in the outer radius for T7 phage.

The thickness of shell structures is highly correlated with the relative fall-off in diffraction ring intensity vs. s. Since any departure from spherical symmetry, dynamic changes in particle shape, and the

resolution limit would all tend to increase apparent shell thickness, resulting electron density profiles indicate an upper limit to the actual shell thickness. The inner and outer radii are characteristic of the shell structures, and are useful for internal comparison between shells, but do not determine the actual boundary of shell protein, where, for example, apparently smooth particles may have projecting tips as in T2 phage (Branton and Klug, 1975). Such details would not be represented in the half-height, or step-function radii.

The effects of resolution cutoff also give rise to extraneous artifactual ripples in the determined electron density functions of Fig. 6. To test the adequacy of a simple step-function density model for the shell structures (capsids II and IV), two parameter model structures were generated in which (*a*) $\rho(r) = 0$ for $r < R_i$, $r < R_o$; and (*b*) $\rho(r) = 1$ for $R_i < r < R_o$. The parameters R_o and R_i were iteratively refined to minimize the function

$$\Delta = \int \| F_o(s)| - k|F_c(s)\| |s^2| ds / \int |F_o(s)\| s^2| ds$$

for all except the zero and first maxima of the transforms. $F_c(s)$ is the calculated transform of the step-function density and k is a least-squares refined scale factor. The value of Δ was refined to a minimum value of 19–25% with the data $f(s)$ that was used to calculate density profiles, and to 12% for data $F'_o(s)$ that had been smoothed (used only for this comparison) to eliminate noise components of wavelength <0.002 Å^{-1} in $F_o(s)$. Such components cannot arise from features contained within the particle, and are due to the film grain, scanning spot dimensions, etc. The resolution limited transform of $F_c(s)$; $[\rho_c(r)]$ was compared with $\rho(r)$ by calculation of $\Delta\rho(r) = |\rho(r) - \rho_c(r)|$, spherical integration of $\Delta\rho(r)$, and of $\rho(r)$. The residual $\int \Delta\rho(r)\, d_V / \int |\rho(r)|\, d_V$ was ~10% (9.5% for capsid II, 10.5% for capsid IV), which showed that the single step-function approximation accounts for ≥90% of the spherically

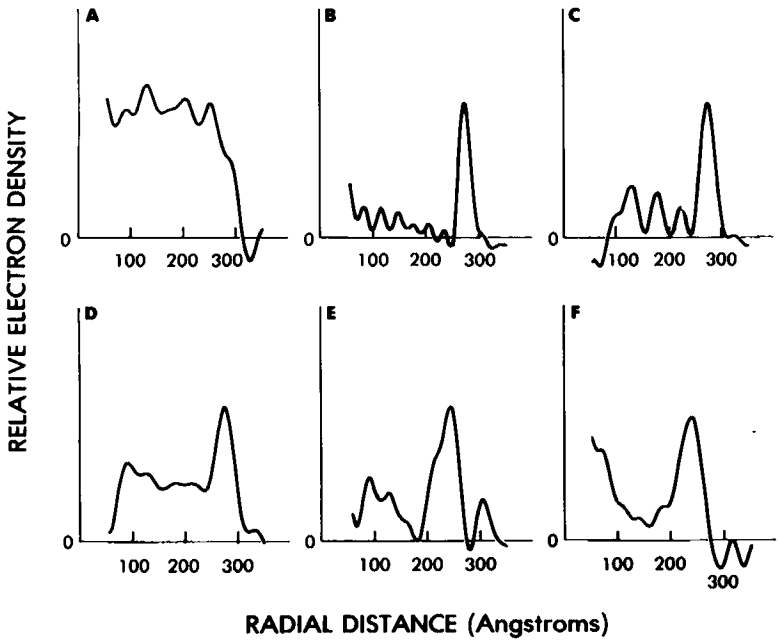

FIGURE 6 Radial electron density profiles. (*A*) T7 phage, (*B*) capsid II, (*C*) capsid IVB, (*D*) capsid I (unfixed), (*E*) wild-type capsid I (fixed), (*F*) Am 5 capsid I (fixed). These profiles are generated by a spherical Fourier transform (see text) of the structure factor profiles shown in Fig. 5. For the purposes of this plot, an exponential cutoff of the form $F' = Fe^{-s^2C}$ has been used to minimize Fourier cutoff ripples. The value chosen for C resulted in a diminution of ≤30% of the intensity of the outermost maximum with respect to the central maximum. No cutoff was employed to arrive at distances reported in Table I.

symmetric electron density. Small variations in density across the shell, lack of spherical symmetry and presence of the tail in capsid IVB can account for all remaining inadequacy of the two parameter models.

RESULTS

Radial electron densities determined are shown in Fig. 6. Radii determined for the models are listed in Table I along with the resolution of each profile. The lowest resolution profile extended to 47 Å (for capsid I, unfixed; eleven observed orders of diffraction), and the highest resolution profile (capsid II) was observable to beyond 30 Å (17 orders of diffraction).

T7 Phage

Bacteriophage T7 has an icosahedral head and a short tail (Fraser and Williams, 1953; Serwer, 1977; Fig. 2 *a*). At 40 Å resolution $\rho(r)$ for T7 phage (Fig. 6 *a*) is roughly constant out to the edge of the phage, and the diffraction pattern is best fit by a solid sphere of radius 301 ± 2 Å, of total volume 11.4 ± 0.4 × 10^{-17} ml. At the outer periphery is a shoulder contributing ~5 Å more to the apparent radius, which we presume arises from either vertices of the polyhedral head or the phage tail.

Empty Capsids with Bacteriophage-like Envelopes

DNA is removed from the T7 envelope by temperature shock to give either capsid IVA (tail −) or IVB (tail +) (see Fig. 1). Capsid II has been shown to be a DNA packaging intermediate with an envelope indistinguishable by electron microscopy from the envelope of capsids IV (Fig. 1). A cylindrical core sometimes present in capsid II disintegrates during storage (Serwer, 1976) and only 15% of the capsid II particles had visible cores at the time diffraction experiments were carried out. The density profiles for capsids II and IVB are identical within experimental limitations (Fig. 6 *b*, *c*) and have peak density at a radius of

TABLE I
CHARACTERISTIC RADII FOR T7 PHAGE AND CAPSIDS

Species	Peak radius*	Shell thickness	Shell radii‡		Orders	Resolution
			Outer	Inner		
		(Å)				(Å)
Native T7	249		301		14	39.7
Capsid II	275	23	286	263	14	36.8
	273	20	283	263	17	30.0
Capsid IVB	274	30	289	259	12	41.1
Capsid I (unfixed)	274	37	292	255	11	47.0
Capsid I (fixed)	247	52	261	209	12	38.7
Capsid I (fixed) from polymerase minus mutants.	243	53	262	209	16	35.0

*Radius of peak electron density in the profile. Errors are estimated to be ±2 Å.
‡Shell radii are defined by refinement of step function models. These values are similar to the radii of half peak height in the profile. This is an arbitrary definition which represents a mean characteristic density at that radius. Lower density material could be present outside the mean radii.

274 ± 2 Å. The apparent difference in shell thickness may reflect the difference in resolution of each profile. The thickness for capsid II, however, at 30-Å resolution is determined from model refinement, or from radius at half peak height to be ~20–30 Å thick. This is an upper limit to the apparent mean shell thickness.

Internal Volume and Contents of T7 Phage

From quantitative densitometry of SDS polyacrylamide gels (Serwer, 1980) the volume occupied by the anhydrous protein in the envelope of capsid II is estimated to be $2.2 \pm 0.2 \times 10^{-17}$ ml. This is close to the volume $1.9–2.2 \times 10^{-17}$ ml calculated with the step-function radii. Thus, the protein of the T7 envelope must be very tightly packed. If the volume occupied by the coat protein were the same in whole phage and capsid II or IV, the inner radius of the T7 envelope would enclose a volume of $9.4 \pm 0.3 \times 10^{-17}$ ml. If one subtracts from this the volume estimated from electron micrographs of the cylindrical core, 0.2×10^{-17} ml, the volume available to DNA would be $9.2 \pm 0.3 \times 10^{-17}$ ml. The molecular weight of T7 DNA is 26.5×10^6 (McDonell et al., 1977). A high-angle reflection of spacing 23.6 Å is identified with an hexagonally packed lattice of DNA strands in the phage (North and Rich, 1961), which implies a DNA-DNA spacing of 27.3 Å in a lattice of cross sectional area 643 Å^2. Thus, the volume occupied by T7 DNA if one assumes for DNA an average mol wt of 662/base pair and an interbase pair spacing of 3.4 Å, is 8.8×10^{-17} ml, close to the total available volume in the head.

Prohead Capsid I

Electron microscopy of capsid I (see Fig. 1) suggests that it is a hollow spherical shell with an internal core and a thicker envelope than the envelopes of capsids II and IV (Serwer, 1976; Fig. 3 *b*). Capsid I also contains more of proteins P9 and P19 (T7 proteins are referred to by "P," followed by the number of the protein's gene; Studier, 1972) than are found in capsids II, IV or phage T7 (Serwer, 1976; Roeder and Sadowski, 1977). Capsid I particles from wild-type T7 lysates and from 5 Am lysates are similar in appearance and in protein composition (P. Serwer, unpublished observations). However, after pelleting for electron microscopy, capsid I is converted to a capsid II-like particle that sometimes had additional, amorphous, and internal material. The radial electron density profile for the pelleting-induced conversion of wild-type capsid I (Fig. 6 *d*) shows the close similarity of the density peak around the 274-Å radius to that of capsid II. The profile also indicates material (probably P9) distributed within the expanded precursor capsid.

The conversion induced by pelleting was blocked by fixing in glutaraldehyde (see Materials and Methods) before, but not after, pelleting. The density profiles for fixed capsid I from a 5 Am preparation (Fig. 6 *f*) and from a wild-type preparation (Fig. 6 *e*) both show peak density at $R = 245 \pm 2$ Å, and indicate a 53-Å thickness, a thicker outer shell than seen in capsid II or IV at the same resolution. In addition, there is material at low radius, presumably because of the core. Calculations using the radii derived show the volume of protein in the outer shell to be 3.6×10^{-17} ml. It would enclose a volume of 3.8×10^{-17} ml, minus the volume of the core of capsid I from electron micrographs 0.2×10^{-17} ml or 3.6×10^{-17} ml. Thus, the net internal expansion between capsid I and whole phage is $\sim 5.6 \times 10^{-17}$ ml, or a factor of ~2.5.

DISCUSSION

Bacteriophage T7 has a radius of 301 ± 2 Å. This is ~30% larger than the radius of unflattened T7 prepared for electron microscopy by negative or positive staining with uranyl acetate, freeze-drying, or thin sectioning (Serwer, 1977, and references therein). Although the reason for this difference in size is not known for certain, it probably results from dehydration during preparation for electron microscopy. Therefore, similar shrinkage is a possibility during the preparation of other viruses for electron microscopy, and dimensions from electron microscopy should be used with appropriate caution. Flattening of viruses during negative staining may obscure shrinkage (Serwer, 1977) and is the likely cause for the comparatively accurate radii obtained by this technique (reviewed in Earnshaw et al., 1978*a*). Evidence for unequal shrinkage of the protein and nucleic acid of bacteriophages T7 and T5 during negative staining has been presented (Serwer, 1979) and distortion in the arrangement, as well as dimensions, of nucleoprotein complexes may be caused by negative staining. This is a more serious problem with nonsymmetric objects such as ribosomes.

Capsid I has a smaller radius than capsid II, which indicates an increase in the internal volume during DNA packaging. It has been suggested that this increase in volume produces a pressure difference that assists T7 DNA packaging (Serwer, 1975, 1980). Bacteriophage T7 has a 5% larger radius than capsid II, however, and the radius of the capsid of bacteriophage T7 decreases after ejection of DNA (see below), which suggests that expansion of the capsid to the size of bacteriophage T7 is energetically unfavorable if only the energy components of the capsid are considered. This indicates that either expansion is not the sole source of energy for DNA packaging (i.e., that the above hypothesis is either incomplete or incorrect) or that the T7 capsid achieves as yet undetected states (a hyperexpanded state, perhaps) during DNA packaging.

The finding of a smaller radius for capsid I than bacteriophage T7 is qualitatively similar to findings for bacteriophage P22 and an apparently analogous P22 capsid (Earnshaw et al., 1976). But, the finding that the empty heads, capsid II, and capsid IVB have a smaller radius than bacteriophage T7, is different from the findings with an analogous P22 capsid in Earnshaw et al. (1976). It must be questioned whether the difference in size between bacteriophage T7 and capsid IVB is an artifact due to limitations of the method, or is a true indication of a further structural change that occurs in the head protein on successful packaging of DNA. It is extremely unlikely that the difference is artifactual for the following reasons. The mean outer diameter of phage T7, 301 ± 2 Å, is very well determined independent of resolution by the positions of maxima and minima in the T7 diffraction pattern. Likewise, the peak-density radius is equally well determined at 273–275 Å in capsids II, IV, and even in expanded capsid I. The thickness of these shell structures, more open to artifact, is essentially resolution limited in the profiles, and also may reflect up to 3.7% maximum expected variations in the actual radius of head proteins in an icosahedral head. Nevertheless, the thickness in the profiles or the step-function models represent a maximum value for the actual shell thickness. For the outer diameter of any of the empty head structures to reach that of whole phage would require a 100% error in the determined thickness. We conclude both from the radii and from the character of the density profiles that there is a structural transition between the protein capsid of bacteriophage T7 and capsid IVB corresponding to a reduction of 5% in radius and 15% in volume when DNA is not present.

The organization of DNA within several DNA bacteriophages appears to be very similar, as is indicated by the diffraction ring of spacing 23.6 Å in T7 also observed in phages T2 (23.8 Å) and λ (23.6 Å) (North and Rich, 1961), and later observed in P22 (23.8 Å, Earnshaw et al., 1976, 1977) and $\phi 29$ (23.8 Å, Subirana et al., 1979). (It is 22.9 Å in T4 [Earnshaw et al., 1978*b*], which has unusually modified cytosine bases [Lehman and Pratt, 1960], although T2 also has modified cytosines and both kinds of DNA are glycosylated.) Using deletion mutants of λ phage, Earnshaw and Harrison (1977) showed that the ~24-Å interplanar spacing varied by ~9% (from 23.6 to 25.8 Å) when up to 22% of the DNA was deleted. They argued that the increase in mean intersegment spacing compensated for about two-thirds of the deleted DNA within a constant protein head structure. The finding of interplanar DNA spacings in the range 23.6–23.8 Å in five phages suggests that the head volume available to DNA is either extremely well tuned to a common hydration and packing arrangement for a given amount of phage DNA, or that the head volume can rather precisely define the amount of DNA to be packaged. The volume available for DNA in T7 ($9.2 \pm 0.3 \times 10^{-17}$ ml) is very close to the volume computed for the T7 genome with 23.6-Å interplanar spacing ($\sim 8.8 \times 10^{-17}$ ml); thus, essentially all of the available volume is used.

The angular width of the 23.6-Å reflection is $\Delta s = 1/132$ Å (full width at half-maximum intensity) and this width is correlated directly with integrity of an ordered hexagonal lattice of parallel DNA strands with DNA-DNA spacing of 27.25 Å (North and Rich, 1961). It has generally been viewed (see, for example, Earnshaw and Harrison, 1977; Earnshaw et al., 1978*b*) as arising from domains of certain mean size (119 ± 10 Å in T7; North and Rich, 1961) that each contain a perfectly ordered DNA lattice. Furthermore, since this reflection is always modulated by ripples of wavelength ~1/head radius it has been suggested that DNA strands on one side of the head are ordered with respect to DNA strands on the other (Earnshaw and Harrison, 1977). The width of the ~24-Å reflection can equally well be explained by a lattice in which the DNA-DNA spacing is subject to statistical variation. Although no distinction between this and the 'domain' description can yet be made, we have calculated the standard deviation $\pm\delta$ Å in DNA-DNA distance within an hexagonal lattice of parallel DNA rods throughout the phage head, which would by itself account for the broadening as 27.3 ± 2.2 Å. Although we regard this a more plausible interpretation, it is nevertheless only an upper limit to the variation since it explains the line broadening when no domain size effect is assumed; factors such as phage head shape, different curvature for DNA strands, or lattice defects must account for some of the broadening. Further, DNA strands on opposite sides of the head must therefore be coherently organized, since they are only 21/22 lattice rows apart, i.e., 519 ± <10 Å. On the other hand, the domain-size calculation gives only a lower limit to the domain size, since it assumes perfect ordering within domains, and it gives no feeling for the amount of disorder or order in the lattice. The radial scattering amplitude $F(s)$ from T7 phage is well represented by a normal distribution, which has a standard deviation of $\sigma_s = 1/220$ Å. (See Bracewell, 1978)

The mean DNA-DNA spacing in all phages so far analyzed ranges from 27.3 to 27.5 Å, and is essentially the same as found in crystalline DNA (27.6 Å, Giannoni et al., 1969; Lerman et al., 1976). Packaged DNA has always been found in the B form and has a hydration of 1.5 g of water/g of DNA. A model in which DNA is spooled around a common axis was proposed by Richards et al. (1973), based on microscopy of disrupted T4 phage, and

further support for such a model was presented by Earnshaw et al. (1978*b*). In T2 (North and Rich, 1961) and in T4, the spool axis was shown to lie more nearly perpendicular to the tail axis than parallel, and the phage heads were elongated parallel to the tail axis. The protein core in T7 (Serwer, 1976) may provide a central spool organization, although in this case the spool axis would have to lie parallel to the tail, and the packaging mechanism would need to be somewhat different to account for spooling around a different axis, within the much more isometric head of T7.

The hydration we compute for T7 DNA is 1.5 g H_2O/g of DNA, essentially identical to the values of 1.5 and 1.54 based on the electron density and packing parameters, respectively, for the DNA in all other phages (Earnshaw and Casjens, 1980).

The help of Dr. W. B. Wood is gratefully acknowledged.

This work was carried out with the support of the National Institutes of Health (grant GM24485 to Dr. Stroud), the National Science Foundation (grant PCM80-21433 to Dr. Stroud), and the U. S. Public Health Service (grant A102938 to Dr. W. B. Wood and grant GM 24365 to Dr. Serwer).

Received for publication 5 February 1981 and in revised form 24 July 1981.

REFERENCES

Adler, S., and P. Modrich. 1979. T7-Induced DNA polymerase: characterization of associated exonuclease activities and resolution into biologically active subunits. *J. Biol. Chem.* 254:11605–11614.

Anderegg, J. W., P. H. Geil, W. W. Beeman, and P. Kaesberg. 1961. An x-ray scattering investigation of wild cucumber mosaic virus and a related protein. *Biophys. J.* 1:657–667.

Anderegg, J. W., M. Wright, and P. Kaesberg. 1963. An x-ray scattering study of bromegrass mosaic virus. *Biophys. J.* 3:175–182.

Bancroft, F. C., and D. Freifelder. 1970. Molecular weights of coliphages and coliphage DNA. I. Measurement of the molecular weight of bacteriophage T7 by high speed equilibrium centrifugation. *J. Mol. Biol.* 54:537–546.

Bracewell, R. 1978. The Fourier Transform and its Applications. McGraw-Hill Publications, New York. 2nd edition. Chapt. 12, pp. 241–274.

Bragg, W. L., and M. F. Perutz. 1952. The structure of haemoglobin. *Proc. Roy. Soc. Ser. A* 213:425–435.

Branton, D., and A. Klug. 1975. Capsid geometry of bacteriophage T2: a freeze-etching study. *J. Mol. Biol.* 92:559–565.

Casjens, S., and J. King. 1975. Virus assembly. *Annu. Rev. Biochem.* 44:555–611.

Earnshaw, W., S. Casjens, and S. C. Harrison. 1976. Assembly of the head of bacteriophage P22: x-ray diffraction from heads, proheads, and related structures. *J. Mol. Biol.* 104:387–410.

Earnshaw, W. C., and S. C. Harrison. 1977. DNA arrangement in isometric phage heads. *Nature (Lond.).* 268:598–602.

Earnshaw, W., J. King, and F. Eiserling. 1978*a*. The size of bacteriophage T4 in solution with comments about the dimension of virus particles as visualized by electron microscopy. *J. Mol. Biol.* 122:247–253.

Earnshaw, W. C., J. King, S. C. Harrison, and F. Eiserling. 1978*b*. The structural organization of DNA packaged within the heads of T4 wild-type isometric and giant bacteriophages. *Cell.* 14:559–568.

Earnshaw, W. C., R. Hendrix, and J. King. 1979. Structural studies of bacteriophage lambda heads and proheads by small angle x-ray diffraction. *J. Mol. Biol.* 134:575–594.

Earnshaw, W. C., and S. Casjens. 1980. DNA packaging by the double-stranded DNA bacteriophage. *Cell.* 21:319–331.

Fraser, D., and R. C. Williams. 1953. Details of frozen-dried T3 and T7 bacteriophage as shown by electron microscopy. *J. Bacteriol.* 65:167–182.

Giannoni, G., F. J. Padden, Jr., and H. D. Keith. 1969. Crystallization of DNA from dilute solution. *Proc. Natl. Acad. Sci. U.S.A.* 62:964–971.

Guinier, A., and G. Fournet. 1955. Small Angle Scattering of X-rays, John Wiley & Sons, New York. 2–82.

Harrison, S. C. 1969. Structure of tomato bushy stunt virus. I. The spherically averaged electron density. *J. Mol. Biol.* 42:457–483.

Hori, K., D. F. Mark, and C. C. Richardson. 1979. DNA polymerase of bacteriophage T7. *J. Biol. Chem.* 254:11591–11597.

Jack, A., and S. C. Harrison. 1975. On the interpretation of small-angle x-ray solution scattering from spherical viruses. *J. Mol. Biol.* 99:15–25.

Kellenberger, E., and J. Séchaud. 1957. Electron microscopical studies of phage multiplication. II. Production of phage-related structures during multiplication of phages T2 and T4. *Virology.* 3:256–274.

Kistler, J., U. Aebi, L. Onorato, B. Ten Heggeler, and M. K. Showe. 1978. Structural changes during the transformation of bacteriophage T4 polyheads: characterization of the initial and final states by freeze-drying and shadowing fab fragment-labeled preparations. *J. Mol. Biol.* 126:571–589.

Lehman, I. R., and E. A. Pratt. 1960. On the structure of the glucosylated hydroxymethyl cytosine nucleotides of coliphages T2, T4, T6. *J. Biol. Chem.* 235:3254–3259.

Lerman, L. S., L. S. Wilkerson, J. H. Venable, Jr., and B. H. Robinson. 1976. DNA packaging in single crystals inferred from freeze-fracture-etch replicas. *J. Mol. Biol.* 108:271–293.

Lowry, O. H., N. J. Rosebrough, A. L. Farr, and R. J. Randall. 1951. Protein measurements with the folin phenol reagent. *J. Biol. Chem.* 193:265–275.

McDonell, M. W., M. N. Simon, and F. W. Studier. 1977. Analysis of restriction fragments of T7 DNA and determination of molecular weights by electrophoresis in neutral and alkaline gels. *J. Mol. Biol.* 110:119–146.

Mencik, Z. 1974. Iterative deconvolution of smeared data functions. *J. Appl. Cryst.* 7:44–50.

Murialdo, H., and A. Becker. 1978. Head morphogenesis of complex double-stranded DNA bacteriophages. *Microbiol. Rev.* 42:529–576.

North, A. C. T., and A. Rich. 1961. X-ray diffraction studies of bacterial viruses. *Nature (Lond.).* 191:1242–1245.

Richards, K. E., R. C. Williams, and R. Calendar. 1973. Mode of DNA packing within bacteriophage heads. *J. Mol. Biol.* 78:255–259.

Roeder, G. S., and P. D. Sadowski. 1977. Bacteriophage T7 morphogenesis: phage-related particles in cells infected with wild-type and mutant T7 phage. *Virology.* 76:263–285.

Ross, M. J., and R. M. Stroud. 1977. Error analysis in the biophysical applications of a flatbed autodensitometer. *Acta Crystallogr. Sect. A.* 33:500–508.

Serwer, P. 1975. Buoyant density sedimentation of macromolecules in sodium iothalamate density gradients. *J. Mol. Biol.* 92:433–448.

Serwer, P. 1976. Internal proteins of bacteriophage T7. *J. Mol. Biol.* 107:271–291.

Serwer, P. 1977. Flattening and shrinkage of bacteriophage T7 after preparation for electron microscopy by negative staining. *J. Ultrastruct. Res.* 58:235–243.

Serwer, P. 1979. Structural alterations in negatively stained specimens. *Proc. Electron Microscopy Soc. Amer.* 37:354–355.

Serwer, P. 1980. A metrizamide-impermeable capsid in the DNA packaging pathway of bacteriophage T7. *J. Mol. Biol.* 138:65–91.

Serwer, P., and R. H. Watson. 1981. Capsid-DNA complexes bound to monomeric and concatemeric DNA. *Virology.* 108:164–176.

Steven, A. C., E. Couture, U. Aebi, and M. K. Showe. 1976. Structure of T4 polyheads. II. A pathway of polyhead transformations as a model for T4 capsid maturation. *J. Mol. Biol.* 106:187–221.

Studier, F. W. 1969. The genetics and physiology of bacteriophage T7. *Virology.* 39:562–574.

Studier, F. W. 1972. Bacteriophage T7. *Science (Wash. D.C.).* 176:367–376.

Subirana, J. A., J. Lloveras, M. Lombardero, and E. Viñuela. 1979. X-ray scattering of the nonisometric *Bacillus subtilis* ϕ29. *J. Mol. Biol.* 128:101–106.

Tikchonenko, T. I. 1969. Conformation of viral nucleic acids *in situ*. *Adv. Virus Res.* 15:201–290.

Wood, W. B., and J. King. 1979. *In* Comprehensive Virology. H. Fraenkel-Conrat, and R. R. Wagner, editors. Plenum Publishing Corp., New York. 13:581–633.